

Unsteady Turbulent Flow Simulations of the Base of a Generic Tractor/Trailer

Christopher J. Roy[†] and J. Chad Brown[‡]

211 Aerospace Engineering Bldg.
Auburn University, Alabama 36849-5338

Lawrence J. DeChant[§] and Matthew F. Barone[¶]

Sandia National Laboratories^{*}
P. O. Box 5800, MS 0825
Albuquerque, NM 87185-0825

Abstract

Preliminary results are presented for Detached Eddy Simulations (DES) of a generic tractor/trailer geometry at a Reynolds number of 2 million based on the trailer width. The DES simulations are compared to both experimental data and to steady-state Reynolds-Averaged Navier-Stokes (RANS) computations using the Menter $k-\omega$ turbulence model. These comparisons include both time-averaged base pressures and wake velocities. The DES results do not provide improved agreement with the experimental data relative to the steady-state RANS results. The lack of improved agreement is likely due to insufficient mesh refinement.

Introduction

In a typical class 8 tractor/trailer, energy losses due to rolling resistance and accessories increase linearly with vehicle speed, while energy losses due to aerodynamic drag increase with the cube of the speed. At a typical highway speed of 70 *mph*, aerodynamic drag accounts for approximately 65% of the energy output of the engine.¹ Due to the large number of tractor/trailers on the US highways, even modest reductions in aerodynamic

drag can significantly reduce domestic fuel consumption. Lower fuel consumption will result in a reduction in pollution emissions and a reduced dependence on foreign oil.

The most common turbulence modeling approach for engineering applications involves solving the Reynolds-Averaged Navier-Stokes (RANS) equations. With this approach, the effects of the inherently three-dimensional and time-varying turbulent eddies on the mean flow are modeled and not simulated. The *effects* of the turbulence, namely increased transport of momentum and energy, are incorporated via the eddy viscosity and eddy conductivity, respectively. In general, it is desirable to obtain steady-state solutions to the RANS equations; the simulation of unsteady RANS flows may only be valid when there is a clear separation between the unsteady scales and the turbulent scales.

RANS turbulence models were generally developed to solve simple, zero pressure gradient attached flows. These models often fail in the presence of large pressure gradients and/or separated flow regions. While the flow over the major part of a tractor/trailer is attached and therefore amenable to RANS modeling, the flow in the base region involves separation off of the rear end of the trailer. This recirculation zone is generally unsteady, with large-scale turbulent structures shedding from the edges. Accurate prediction of the flow in the base region is important since it determines the pressure on the trailer base. The pressure drag is the primary component of the overall aerodynamic drag for tractor/trailer configurations, and small errors in the predicted base pressures can significantly affect the drag calculations.

The Large Eddy Simulation (LES) approach is becoming a popular technique to model bluff-body flows.

[†] Assistant Professor, E-mail: cjroy@eng.auburn.edu, Senior Member AIAA

[‡] Undergraduate Research Assistant, Student Member AIAA

[§] Senior Member of Technical Staff, E-mail: ljdech@sandia.gov, Member AIAA

[¶] Senior Member of Technical Staff, E-mail: mbarone@sandia.gov, Member AIAA

^{*} Sandia is a multiprogram laboratory operated by Sandia Corporation, a Lockheed Martin Company, for the United States Department of Energy under Contract DE-AC04-94AL85000.

In LES, the larger structures (eddies) in the turbulent spectrum are resolved, and the smaller structures are modeled. This approach is computationally expensive and there are still modeling issues that are being investigated. A subgrid-scale model must be used. The classic subgrid-scale model was introduced by Smagorinsky,² while the dynamic model approach of Germano et al.³ has become very popular. This paper is concerned with wall bounded flows where additional modeling is required near the surface. The unsteady turbulence modeling technique investigated herein is the hybrid RANS/LES model Detached Eddy Simulation (DES) developed by Spalart and co-workers.⁴

The current effort is an extension of prior work by the authors. An earlier study examined the same generic tractor/trailer geometry, but used steady-state RANS models.⁵ The authors have also employed the DES approach to study the flow over a square cross-section cylinder at a Reynolds number of 22,000.⁶ The square cylinder is a geometrically simple, bluff body flow that has been the basis of numerous computational and experimental studies. The current study seeks to extend the prior work using the DES method to a much higher Reynolds number.

Simulation Approach

Simulation Code

The computational fluid dynamics code used herein is SACCARA, the Sandia Advanced Code for Compressible Aerothermodynamics Research and Analysis. The SACCARA code was developed from a parallel distributed memory version⁷ of the INCA code,⁸ originally written by Amtec Engineering. The SACCARA code is used to solve the Navier-Stokes equations for conservation of mass, momentum, energy, and turbulence transport in either 2D or 3D form. Prior code verification studies with SACCARA include code-to-code comparisons with other Navier-Stokes codes^{9,10} and with the Direct Simulation Monte Carlo method.¹¹ These studies provide some confidence that the code is free from coding errors affecting the discretization.

Discretization

The governing equations are discretized using a cell-centered finite-volume approach. The discretization of the convective terms is based on a finite-volume form of Harten and Yee's symmetric TVD scheme.^{12,13} This baseline scheme is modified using a characteristic-based filter which greatly decreases the numerical dissipation in smooth regions of the flow (see Ref. 14 for details). The resulting scheme is second-order accurate with low dissipation in smooth regions. The viscous terms are discretized using central differences. The SACCARA

code employs a massively parallel distributed memory architecture based on multi-block structured grids.

The solver is a Lower-Upper Symmetric Gauss-Seidel scheme based on the works of Yoon et al.¹⁵ and Peery and Imlay,¹⁶ which provides for excellent scalability up to thousands of processors.¹⁷ Second-order accuracy is obtained in the temporal discretization via a sub-iterative procedure. In this approach, the time derivative in the governing equations is discretized with a second-order backward difference. The three-point backward time derivative is added to the steady-state residual, and the solution at time level $n+1$ is iterated until the right-hand side, which includes both the steady-state residual and the time derivative, are driven below a given tolerance.

Turbulence Models

For the simulations results presented herein, the turbulence transport equations are integrated all the way to the vehicle walls, thus no wall functions are employed. In all cases, the distance from the wall to the first cell center off the wall is less than unity in normalized turbulence distance (i.e., $y^+ < 1$).

Steady-State RANS

The steady-state RANS model examined is Menter's hybrid model¹⁸ which switches from a $k-\epsilon$ formulation in the outer flow to a $k-\omega$ formulation near solid walls. Additional details on the RANS solution using the Menter model can be found in Ref. 5.

Detached Eddy Simulation (DES)

The hybrid RANS/LES method developed by Spalart and co-workers (Refs. 4, 19) has been developed the furthest and is called Detached Eddy Simulation, or DES. The DES approach uses the unsteady form of the Spalart-Allmaras one-equation eddy viscosity model²⁰ to provide the eddy viscosity $\nu_T = \mu_T/\bar{\rho}$ for use in the sub-grid scale stress model. The Spalart and Allmaras one-equation eddy viscosity model provides the usual RANS-based eddy viscosity in the boundary layer, but must be modified to the appropriate eddy viscosity for LES outside of the boundary layer. This modification is performed by changing the definition of the distance to the wall d in the destruction term. The distance d is replaced with \tilde{d} , where this new term is defined as

$$\tilde{d} = \min(d, C_{DES}\Delta) \quad (1)$$

Far from the wall, the value of \tilde{d} thus becomes

$$\tilde{d} = C_{DES}\Delta. \quad (2)$$

The local grid spacing is defined as Δ and is equal to the maximum mesh spacing in the three coordinate di-

rections.

$$\Delta = \max(\Delta x, \Delta y, \Delta z)$$

As discussed by Spalart et al.,⁴ when the production term is balanced with the destruction term (at equilibrium), the following is obtained

$$\mu_T = \bar{C}_S^2 \bar{\rho} \Delta^2 \tilde{S}, \quad \bar{C}_S = C_{DES} \sqrt{\frac{C_b k f_v}{C_w k f_w}} \quad (3)$$

where \tilde{S} is related to the magnitude of the strain rate. In the outer part of the boundary layer, \bar{C}_S asymptotes to $\bar{C}_S = 0.29 C_{DES} = 0.19$. The constant C_{DES} is given by Spalart as

$$C_{DES} = 0.65 \quad (4)$$

The DES model thus asymptotes to a Smagorinsky-type LES model in the bluff-body wake assuming sufficient mesh refinement.

Problem Description

The flow over the Ground Transportation System (GTS) model has been investigated experimentally at a Reynolds number Re_W of 2 million by Storms et al.,²¹ where W refers to the width of the trailer base (0.32385 m). A photograph of the GTS mounted in the NASA Ames 7'×10' wind tunnel is presented in Fig. 1. The experimental data set is unique in that it presents both ensemble-averaged surface pressure data (see Fig. 2) as well as multiple planes of instantaneous and ensemble-averaged velocity data in the wake (see Fig. 3) for this high Reynolds number flow.



Fig. 1: Photograph of the GTS geometry in the NASA Ames wind tunnel.

In order to perform the computationally intensive DES simulations, the front of the GTS was truncated along with the wind tunnel wall at $x/W = 2$ as shown in Fig. 4. This figure also shows the Cartesian coordinate system employed, normalized by the trailer width W . Note that the wind tunnel wall as well as the rear posts are included in the simulation. This mesh is composed

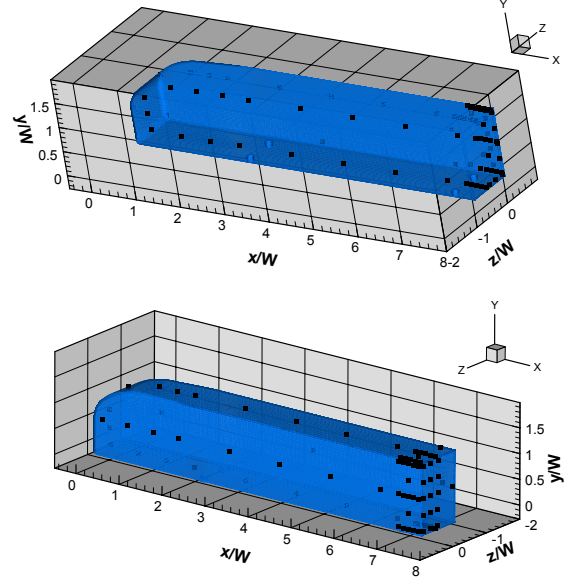


Fig. 2: Locations of experimental surface pressure data.

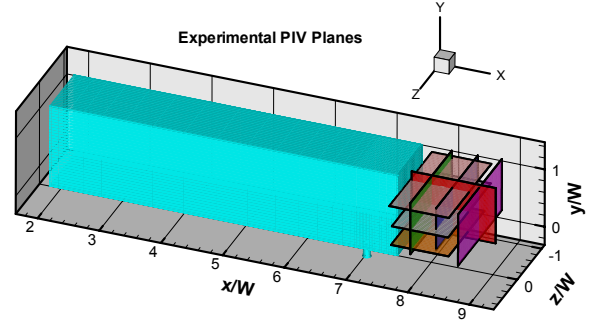


Fig. 3: Location of experimental velocity data planes.

of approximately 4 million grid points and was domain decomposed and run on 32 processors of a Linux cluster.

Boundary Conditions

The inflow boundary employs stagnation values for pressure ($102,653 \text{ N/m}^2$) and temperature (282.1 K) and enforces inflow normal to the boundary. The outflow boundary used a fixed static pressure of $97,700 \text{ N/m}^2$. This back pressure was chosen so that the tunnel wall reference pressure, located at $x/W = 4.47$, $y/W = 2.5882$, $z/W = -4.7$, matched with the experiment. The reference pressure found from the computations was $97,400 \text{ N/m}^2$ (see Fig. 5) which corresponds to a freestream velocity of approximately 91.9 m/s . Slip conditions on velocity are employed on the top and side walls of the wind tunnel, while the lower wind tunnel wall, the GTS surface, and the support posts employ no-slip velocity conditions

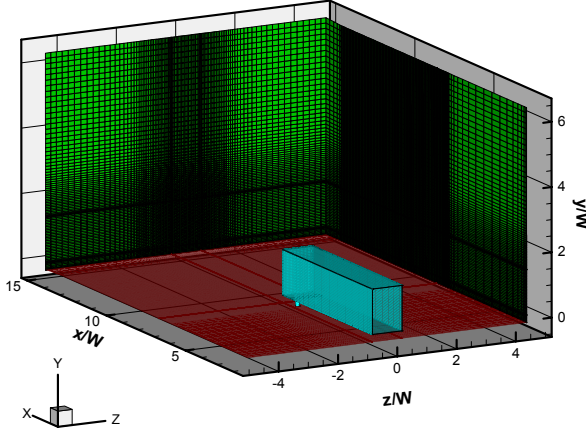


Fig. 4: Computational domain for the truncated GTS model in the simulated wind tunnel.

and assume an adiabatic wall. The freestream eddy viscosity is set at $1 \times 10^{-5} \text{ N}\cdot\text{s}/\text{m}^2$. Solid wall boundary conditions for the turbulence model can be found in Ref. 22.

Characteristic Scales

Time can be normalized by a reference time scale defined as

$$t_{ref} = W/U_{inf} = 0.0033 \text{ s} \quad (5)$$

where U_{inf} is the reference velocity from the simulations. A time history of the reference pressure is given in Fig. 5. The drop in the reference pressure over time is due to a back pressure initially being set to too large of a value. Unless otherwise noted, the simulations employed a dimensionless time step $\Delta t/t_{ref}$ of 0.0012.

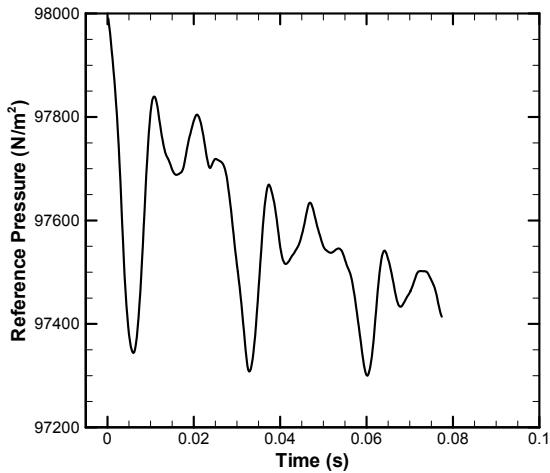


Fig. 5: Reference pressure history from $x/W = 4.47$, $y/W = 2.5882$, $z/W = -4.7$.

Some characteristic length scales are given in Table 1. The extremely fine grid spacing near the wall (Δ_{wall}) is required because the RANS model is integrated to the wall. The maximum grid spacing in the trailer wake (Δ_{wake}) leads to approximately 21 points across the trailer width for this coarse grid case.

Table 1 Characteristic length scales

	Value (m)
Δ_{wall}	6×10^{-6}
Δ_{wake}	0.015
W	0.32385

Numerical Accuracy

Statistical Convergence

It is unclear *a priori* how long the flowfield statistics sampling should be performed before the statistical error becomes sufficiently small. The experiment provides the time history of one unsteady pressure sensor located in the base of the trailer at $y/W = 0.65$, $z/W = 0.46$. This time history is given in Fig. 6 along with the running mean and RMS pressure values. The experimental statistics appear to be converged within $\pm 5 \text{ N/m}^2$ by approximately 0.1 s. The corresponding unsteady pressure from the simulations is presented in Fig. 7. All simulation results presented herein are sampled over a time window of approximately 0.1 s (30 characteristic time periods) for the preliminary results shown here.

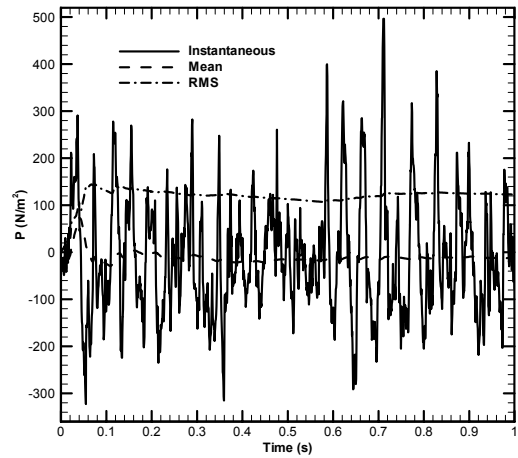


Fig. 6: Time histories of the pressure fluctuations from the experiment.

Iterative Convergence

Prior experience with the iterative convergence levels suggests that a residual reduction of four orders of magnitude is sufficient to make the iterative errors at each

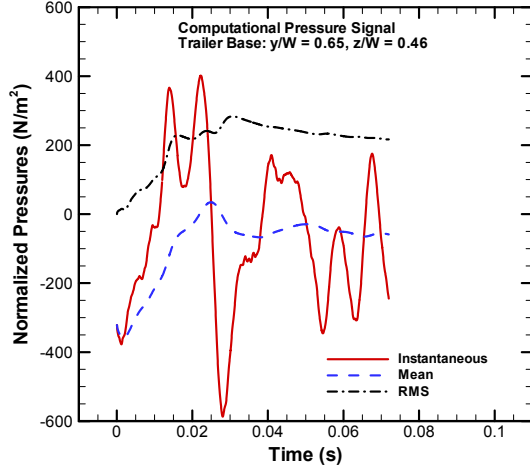


Fig. 7: Time histories of the pressure fluctuations from the DES simulations.

time step negligible. After 10 sub-iterations per time step, most of the zones were converged approximately five orders of magnitude. However, due to the extremely small mesh spacing near the wall, some zones were only converged three orders of magnitude. It is not clear whether this residual reduction is sufficient to allow iterative convergence errors to be neglected.

Discretization Error

The mesh employed in the DES simulations was approximately 4 million grid points. Due to limits on computational resources, the effects of refining the grid and time step have not yet been examined. This deficiency will be addressed in future work.

Results

In this section, results for the steady-state RANS model of Menter and the preliminary results using the DES model are compared with experimental data. These data comparisons include time-averaged streamlines, velocity contour plots, velocity profiles, and surface pressure distributions.

Streamlines and Velocity Contours

Time-averaged streamlines are shown in Fig. 8 along with time-averaged contours of the u - (streamwise-) component of velocity for the experiment, the steady-state Menter $k-\omega$ RANS model, and the DES model. The flow is from left to right, and the aft end of the trailer is also shown in the figures. The experiment shows a large, counter-clockwise-rotating vortex centered at $y/W = 0.4$ near the trailer base. While the corresponding clockwise-rotating vortex is outside of the experimental PIV window, the streamlines appear to suggest that this vortex is centered near the top-right corner of the window ($x/W = 9$, $y/W = 1.2$).

The results for the Menter $k-\omega$ model give a much more symmetric pair of counter-rotating vortices than seen in the experiment (see Fig. 8, middle plot). An outline of the location of the experimental PIV window is also shown in the computational plots. The time-averaged DES results are shown in the bottom of Fig. 8 and show a strong, clockwise-rotating vortex near the base at $y/W = 1$. The streamlines do not form closed circuits in the figure, but spiral towards the center of the vortex. This behavior suggests that the simulation results are not yet statistically converged. Furthermore, the DES simulations, although providing an asymmetric pattern, show a trend opposite to that found in the experiment. The reason for this deviation from the experiment is unknown, but may be caused by insufficient mesh refinement.

Time-averaged streamlines and out-of-plane velocity contours are shown in Fig. 9 for a horizontal, streamwise plane in the wake located at $y/W = 0.36$. The experimental streamlines (top plot) show no coherent recirculation because this plane is below the bottom of the vortex shown in Fig. 8. The vertical velocity contours in the experiment show flow upwards near the center of the PIV window, and downwards near the trailer base.

The Menter $k-\omega$ results shown in the middle of Fig. 9 show vertical velocity contours that are qualitatively similar to those found in the experiment. The streamlines, however, show a clear recirculation zone suggesting that the toroidal vortex ring is located too low in the wake. The DES results also show the counter-rotating vortices (bottom of Fig. 9), but the vertical velocities are opposite that shown in the experiment due to the fact that the flow predicted by the DES model is dominated by the upper, clockwise-rotating vortex in Fig. 8 rather than the lower, counter-clockwise-rotating vortex. The near-symmetry of the DES results about $z/W = 0$ suggests that the DES simulations are nearly statistically converged at this location (at least for the mean quantities).

A similar horizontal, streamwise cut is shown in Fig. 10, however this plane is located higher up on the base at $y/W = 1.06$. In this case, the streamlines from the Menter $k-\omega$ computation appear to match the experiment, however the vertical velocity contours differ. The streamlines for the DES simulations do not show a coherent recirculation pattern due to the fact that this y/W location is above the predicted upper vortex core shown in Fig. 8.

Velocity Profiles

Velocity profiles at three different axial stations ($x/W = 8.0$, $x/W = 8.4$, and $x/W = 8.9$) were extracted from the horizontal streamwise planes given earlier in Fig. 8.

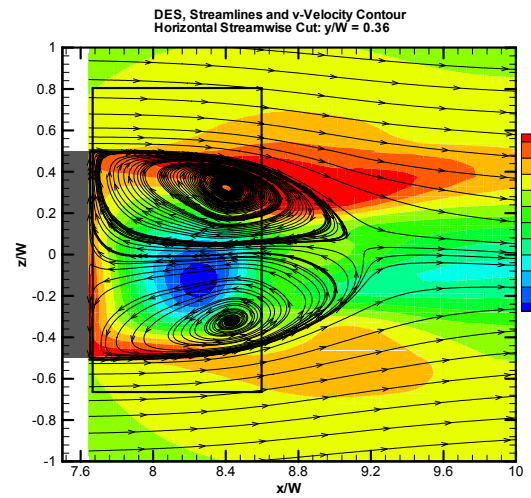
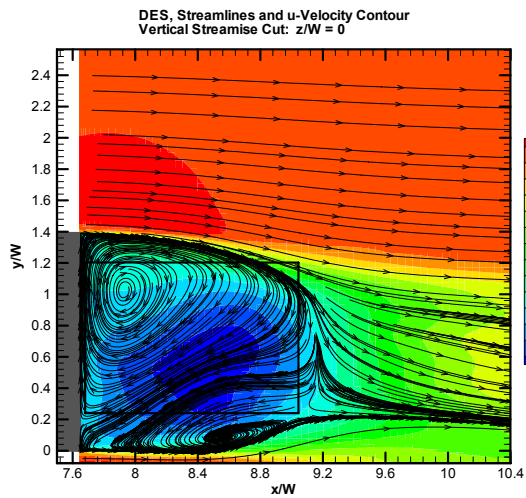
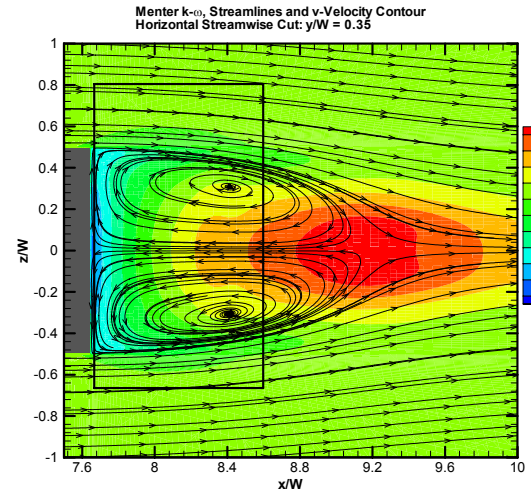
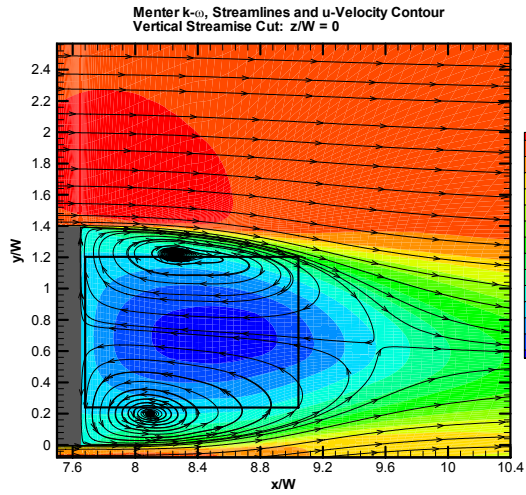
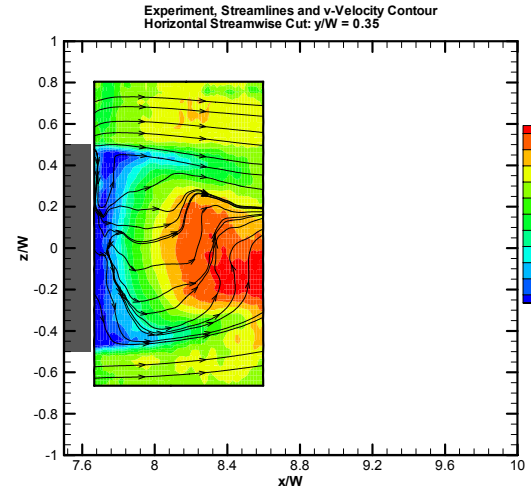
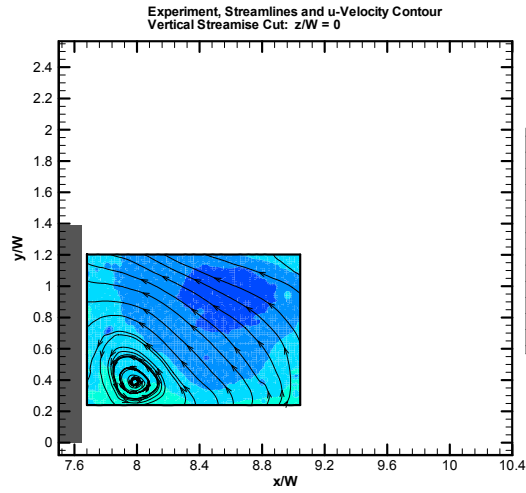


Fig. 8: Streamlines and u-velocity contours at $z/W=0$ for experiment (top), Menter $k-\omega$ (middle), and DES (bottom).

Fig. 9: Streamlines and v-velocity contours at $y/W=0.36$ for experiment (top), Menter $k-\omega$ (middle), and DES (bottom).

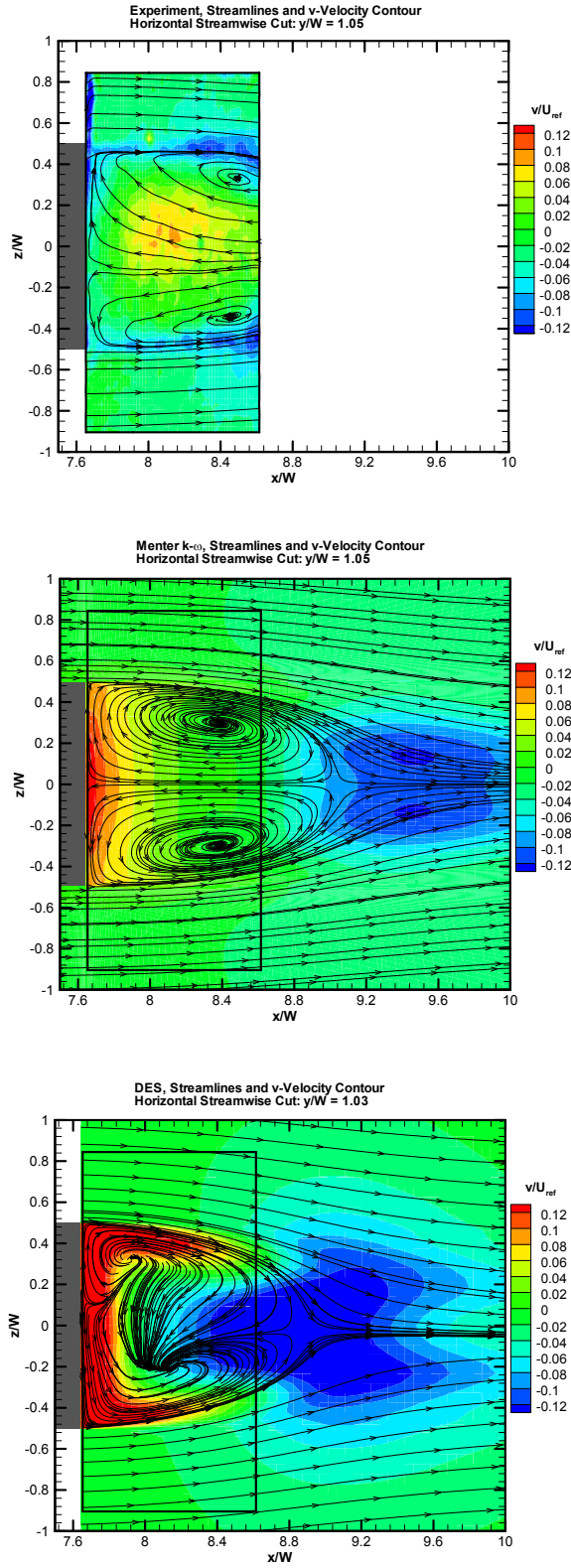


Fig. 10: Streamlines and v-velocity contours at $y/W = 1.03$ for experiment (top), Menter $k-\omega$ (middle), and DES (bottom).

These profiles for u -, v -, and w -components of velocity are presented in Fig. 11. The u -component of velocity is matched reasonable well by both the Menter $k-\omega$ and the DES models (top of Fig. 11). The Menter model also accurately predicts the v -component near the base ($x/W = 8, 0$), but do not agree with the experimental data at the two downstream stations. The DES model does not give accurate predictions of the v -velocity component at any of the three stations. The w -velocity component (bottom plot) shows that the Menter computations are essentially symmetric about $z/W = 0$, however there appears to be some asymmetry in the experiment, as shown by the non-zero w -velocity along the symmetry plane ($z/W = 0$). The non-zero values for the w -velocity predicted by the DES model again suggest that these results are not statistically converged.

Similar velocity profiles are given for the horizontal-streamwise planes at $y/W = 0.36$ (Fig. 12) and $y/W = 1.05$ (Fig. 13). In general, the DES model does not predict the velocities in the wake region as well as the lower-fidelity Menter model. Again, this may be due to mesh refinement issues with the DES model.

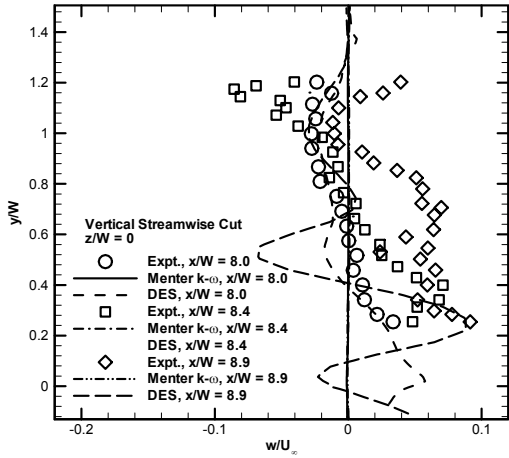
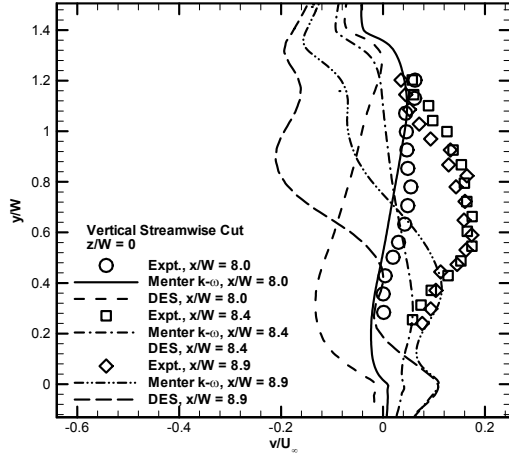
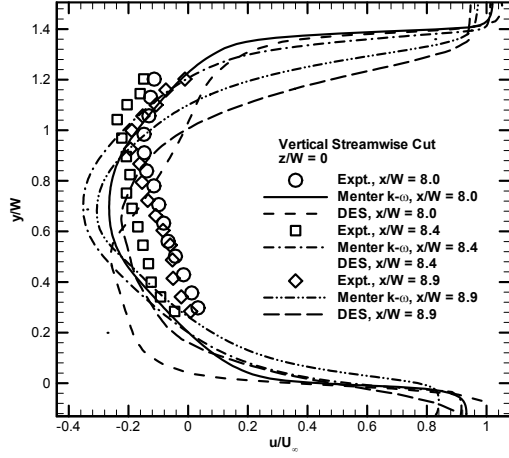


Fig. 11: Profiles of u -velocity (top), v -velocity (middle), and w -velocity (bottom) for different x/W stations at $z/W = 0$.

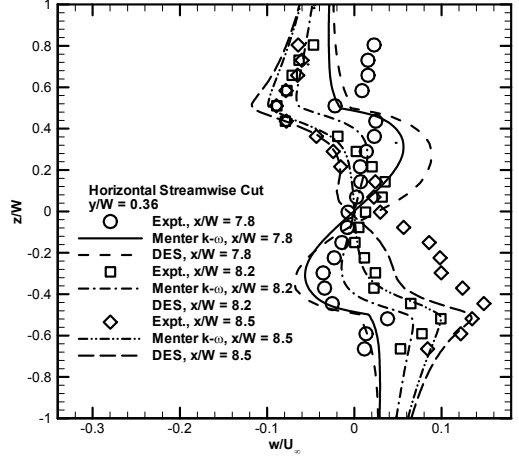
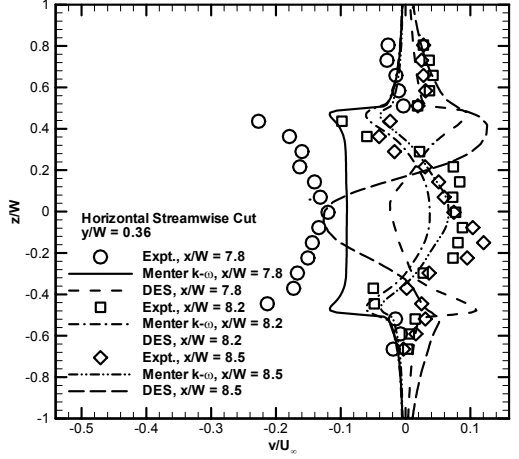
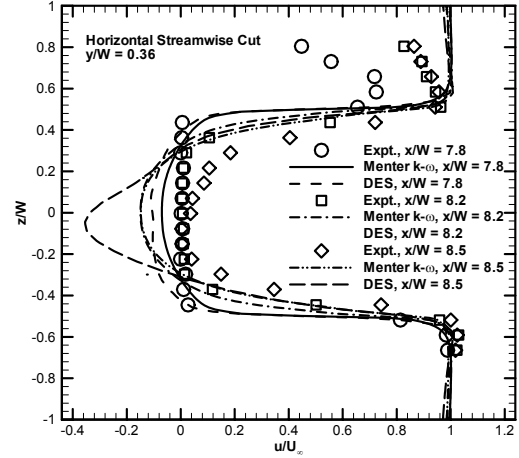


Fig. 12: Profiles of u -velocity (top), v -velocity (middle), and w -velocity (bottom) for different x/W stations at $y/W = 0.35$.

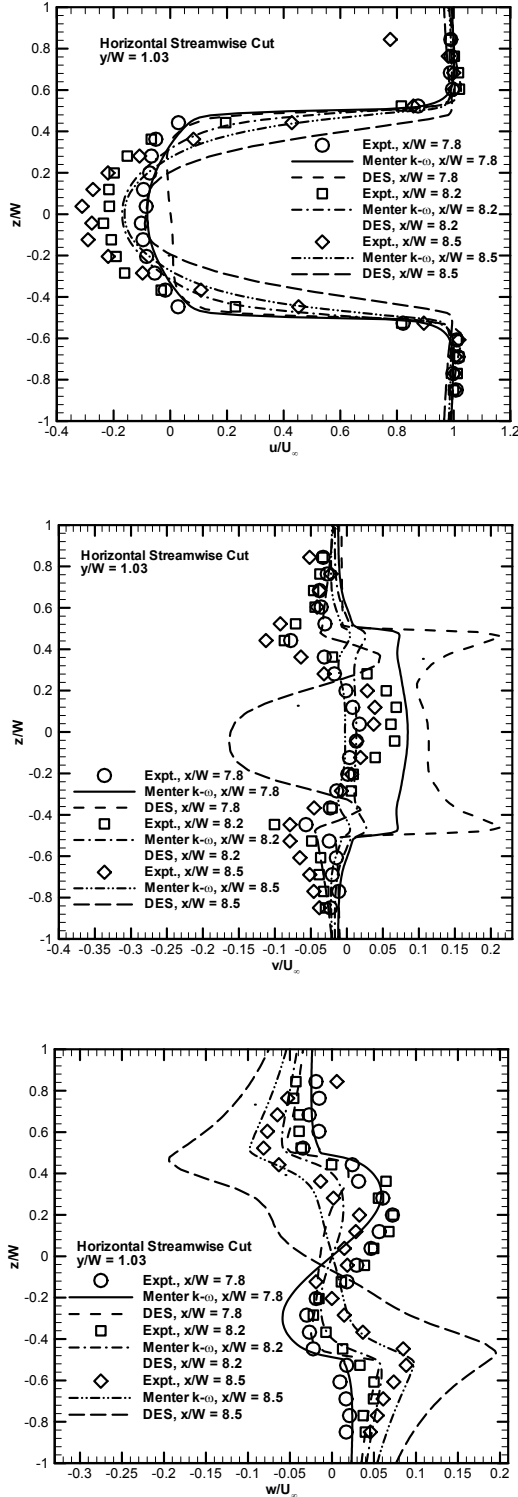


Fig. 13: Profiles of u -velocity (top), v -velocity (middle), and w -velocity (bottom) for different x/W stations at $y/W = 1.03$.

Surface Pressure Distributions

Distributions of pressure coefficient on the trailer base are presented in Fig. 14 for span-wise stations of $z/W = 0$ (the symmetry plane), $z/W = 0.22$, and $z/W = 0.44$. The experiment shows an asymmetrical pressure distribution from top to bottom. The minimum pressure occurs near $y/W = 0.4$ and is due to the proximity to the lower, counter-clockwise-rotating vortex from the top plot of Fig. 8. The Menter results show a much more symmetric pressure distribution from top to bottom as expected due to the symmetric pair of counter-rotating vortices shown in the middle plot of Fig. 8. As expected from the velocity contour plots, the DES model shows the opposite trends than those found in the experiment.

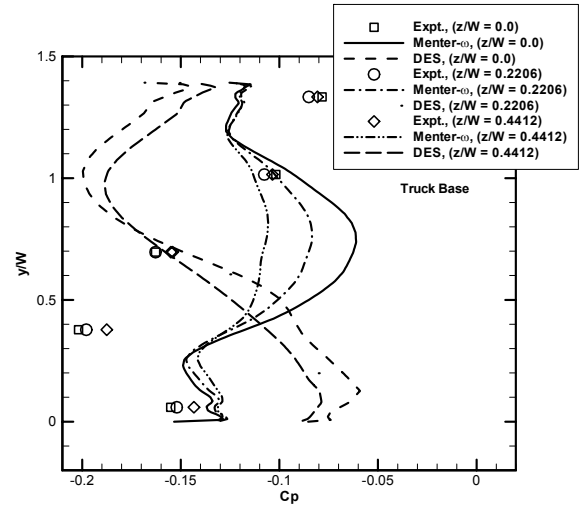


Fig. 14: Pressure coefficient distributions for different z/W stations on the trailer base.

Conclusions

Preliminary results were presented for Detached Eddy Simulations (DES) of generic tractor/trailer geometry at a Reynolds number of 2 million based on the trailer width. The DES simulations were compared to both experimental data and to steady-state Reynolds-Averaged Navier-Stokes (RANS) computations using the Menter $k-\omega$ turbulence model. These comparisons included both time-averaged base pressures and wake velocities. The DES results did not provide improved agreement with the experimental data relative to the steady-state RANS results. The lack of improved agreement was likely due to insufficient mesh refinement.

Acknowledgements

We would like to thank Jeffrey Payne of Sandia National Laboratories for his invaluable help with domain decomposition.

References

1. R. McCallen, R. Couch, J. Hsu, F. Browand, M. Hammache, A. Leonard, M. Brady, K. Salari, W. Rutledge, J. Ross, B. Storms, J. T. Heineck, D. Driver, J. Bel, and G. Zilliac, "Progress in reducing aerodynamic drag for higher efficiency of heavy duty trucks (class 7-8)," SAE Paper 1999-01-2238, 1999.
2. J. Smagorinsky, "General Circulation Experiments with the Primitive Equations, Part I: The Basic Experiment," *Monthly Weather Review*, Vol. 91, p. 99, 1963.
3. M. Germano, U. Piomelli, P. Moin, and W. H. Cabot, "A Dynamic Subgrid-Scale Eddy-Viscosity Model," *Physics of Fluids A*, Vol. 3, No. 7, pp. 1760-1765, 1991.
4. P. R. Spalart, W. H. Jou, M. Strelets, and S. R. Allmaras, "Comments on the Feasibility of LES for Wings, and on a Hybrid RANS/LES Approach," in *Advances in DNS/LES*, Proceedings of the First AFOSR International Conference on DNS/LES, Edited by C. Liu and Z. Liu, Greyden Press, Columbus, OH, 1997.
5. C. J. Roy, J. L. Payne, M. A. McWherter-Payne, and K. Salari, "RANS Simulations of a Simplified Tractor/Trailer Geometry," Conference Proceedings for the Aerodynamics of Heavy Vehicles: Trucks, Buses, and Trains, United Engineering Foundation, Monterey-Pacific Grove, CA, Dec. 2-6, 2002.
6. C. J. Roy, L. J. DeChant, F. G. Blottner, and J. L. Payne, "Bluff-Body Flow Simulations using Hybrid RANS/LES," AIAA Paper 2003-3889, Orlando, FL, June 2003.
7. Wong, C. C., Blottner, F. G., Payne, J. L., and Sotrisno, M., "Implementation of a Parallel Algorithm for Thermo-Chemical Nonequilibrium Flow Solutions," AIAA Paper 95-0152, Jan. 1995.
8. INCA User's Manual, Version 2.0, Amtec Engineering, Inc., Bellevue, WA, 1995.
9. Payne, J. L., and Walker, M. A., "Verification of Computational Aerodynamic Predictions for Complex Hypersonic Vehicles using the INCATM Code," AIAA Paper 95-0762, January 1995.
10. C. J. Roy, M. A. McWherter-Payne, and W. L. Oberkampf, "Verification and Validation for Laminar Hypersonic Flowfields Part I: Verification," *AIAA Journal*, Vol. 41, No. 10, 2003, pp. 1934-1943.
11. C. J. Roy, M. A. Gallis, T. J. Bartel, and J. L. Payne, "Navier-Stokes and DSMC Predictions for Laminar Hypersonic Shock-Induced Separation," *AIAA Journal*, Vol. 41, No. 6, 2003, pp. 1055-1063.
12. Harten, A., "On a Class of High Resolution Total-Variation-Stable Schemes," *SIAM Journal of Numerical Analysis*, Vol. 21, No. 1, 1984, pp. 1-23.
13. Yee, H. C., "Implicit and Symmetric Shock Capturing Schemes," NASA-TM-89464, May 1987.
14. Yee, H. C., Sandham, N. C., and Djomehri, M. J., "Low-Dissipative High-Order Shock-Capturing Methods using Characteristic-Based Filters," *Journal of Computational Physics*, Vol. 150, No. 1, pp. 199-238, March 1999.
15. Yoon, S., and Jameson, A., "An LU-SSOR Scheme for the Euler and Navier-Stokes Equations," AIAA Paper 87-0600, Jan. 1987.
16. Peery, K. M., and Imlay, S. T., "An Efficient Implicit Method for Solving Viscous Multi-Stream Nozzle/Afterbody Flow Fields," AIAA Paper 86-1380, June 1986.
17. Payne, J. L., and Hassan, B., "Massively Parallel Computational Fluid Dynamics Calculations for Aerodynamics and Aerothermodynamics Applications," Proceedings of the 1998 HPCCP/CAS Workshop, NASA/CP-1999-208757, Jan. 1999, pp. 111-116.
18. Menter, F. R., "Two-Equation Eddy-Viscosity Turbulence Models for Engineering Applications," *AIAA Journal*, Vol. 32, No. 8, 1994, pp. 1598-1605.
19. M. Shur, P. R. Spalart, M. Strelets, and A. Travin, "Detached-Eddy Simulation of an Airfoil at High Angle of Attack," 4th International Symposium Engineering Turbulence Modeling and Measurements, May 24-26, Corsica, France, 1999.
20. P. R. Spalart and S. R. Allmaras, "A One-Equation Turbulence Model for Aerodynamic Flows," *La Recherche Aerospatiale*, No. 1, pp. 5-21, 1994.
21. B. Storms, Ross JC, Heineck JT, Walker SM, Driver DM, Zilliac GG, "An Experimental Study of the Ground Transportation System (GTS) Model in the NASA Ames 7- by 10-ft Wind Tunnel," NASA TM-2001-209621, 2001.
22. C. J. Roy and F. G. Blottner, "Methodology for Turbulence Model Validation: Application to Hypersonic Flows," *Journal of Spacecraft and Rockets*, Vol. 40, No. 3, 2003, pp. 313-325.